Extreme Spatial Dispersion in Nonlocally Resonant Elastic Metamaterials

Aleksi Bossart* and Romain Fleury†
Laboratory of Wave Engineering, Ecole Polytechnique Fédérale de Lausanne, 1015 Lausanne, Switzerland

(Received 16 September 2022; accepted 24 April 2023; published 19 May 2023)

To date, the vast majority of architected materials have leveraged two physical principles to control wave behavior, namely, Bragg interference and local resonances. Here, we describe a third path: structures that accommodate a finite number of delocalized zero-energy modes, leading to anomalous dispersion cones that nucleate from extreme spatial dispersion at 0 Hz. We explain how to design such zero-energy modes in the context of elasticity and show that many of the landmark wave properties of metamaterials can also be induced at an extremely subwavelength scale by the associated anomalous cones, without suffering from the same bandwidth limitations. We then validate our theory through a combination of simulations and experiments. Finally, we present an inverse design method to produce anomalous cones at desired locations in k space.

DOI: 10.1103/PhysRevLett.130.207201

In traditional metamaterials, local resonances introduce a flat band that hybridizes with the background dispersion, thereby opening a polariton band gap [1]. When two such gaps overlap [Figs. 1(a) and 1(b)], one having negative effective density [2] and the other negative bulk modulus [3], a "doubly negative" range arises, in which waves propagate with opposite phase and group velocities [4–6]. This property is associated with spatial dispersion [7,8] and provides a mechanical realization of negative refraction [9,10]. While metamaterials were initially electromagnetic [11,12], they have since flourished in acoustics [13–15], thermal physics [16], and mechanics [17–21], merging with auxetic materials [22,23]. Long-range interactions have recently been shown to extend the capabilities of metamaterials, either through radiative coupling [24] or with explicit beyond-next-neighbor connectors [25–27]. Such couplings induce local minima in the dispersion branches, called rotons [28,29].

We propose a distinct path that relies neither on local resonances nor on long-range coupling, while inducing hallmark properties of metamaterials over large-frequency bands. Our inspiration comes from "interlaced wire media" [30,31], which consist of sets of space-spanning, fully connected meshes of metallic wires that interlace without direct contact, thereby allowing for differences in static electric potential between their large disconnected components. This interlacing pattern induces anomalous dispersion cones at symmetric points of the Brillouin zone [30]; consequently, interlaced wire media exhibit unusual electromagnetic wave properties down to the static regime, such as broadband negative refraction.

Here, we identify the abstract ingredients underlying the physical properties of such wave media, which we propose to call *nonlocally resonant metamaterials*. Indeed, they rely on delocalized eigenmodes at zero frequency, or nonlocal resonances, to parallel the traditional terminology. This paradigm allows us to expand their scope to the elastic realm, providing an inverse-design procedure and experimental validation.

In elasticity, a delocalized zero-frequency mode consists of a locally rigid deformation (or "mechanism") that spans the whole medium. More precisely, we require this resonance to have a well-defined wave vector $\mathbf{k_R}$, isolated in k space. Indeed, if the immediate neighborhood of $\mathbf{k_R}$ also hosted zero-energy modes, we could construct zero-frequency wave packets, thereby making the resonance local. In contrast, an isolated $\mathbf{k_R}$ guarantees sample-spanning spatial extension in the form of a Bloch wave. Crucially, the continuity of the spectrum ensures that an anomalous cone nucleates from $\mathbf{k_R}$, as in Fig. 1(c). Here, "anomalous" refers to dispersion cones not associated with the translation symmetries that underlie standard elastic waves. A trailblazing geometry that fits these stringent requirements is the counterrotating squares structure, introduced to model displacive phase transitions in minerals [32,33]. Similar mechanisms were also described in a topological study of the deformed square lattice [34]. Here, we provide a general paradigm to understand and inversely design extremely nonlocal elastic resonances. We theoretically and experimentally explore the wave physics of nonlocally resonant elastic metamaterials.

We begin by picturing the metamaterial of Fig. 1(d) as a collection of oscillating masses (blue diamonds) connected by springs (dark bars). In zero-frequency oscillations, only rigid motions are possible; not a single spring can be stretched. Rigid translations of the entire structure fulfill this criterion; such zero-frequency modes correspond to in-plane transverse and longitudinal elastic waves in the limit of infinite wavelength, which confines them to the Γ point. For sufficiently high connectivity, these are the only

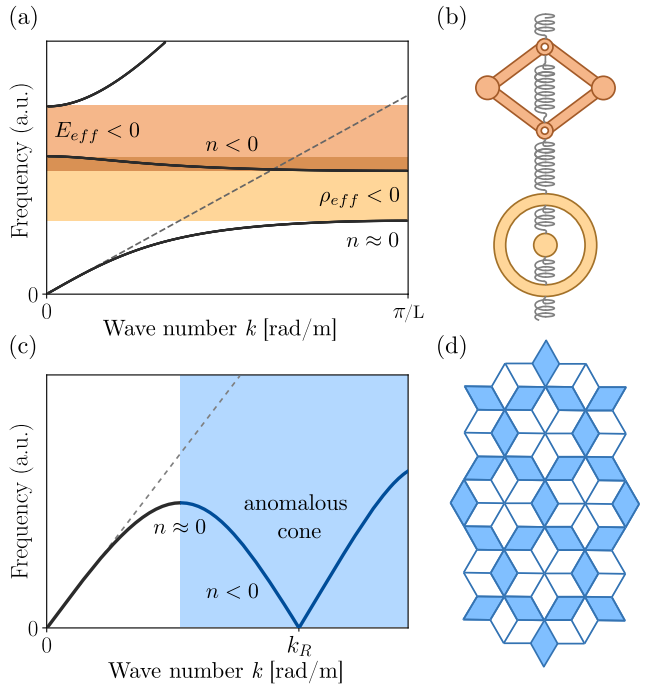

FIG. 1. (a) Dispersion of a locally resonant metamaterial, with the ranges of negative bulk modulus and density highlighted in orange and yellow, respectively. The domain in which they overlap (brown region) hosts a band with negative group velocity. (b) 1D spring-mass chain giving rise to the dispersion in (a), with the mechanisms responsible for effective negative compressibility and density colored accordingly. (c) On the other hand, the dispersion of a nonlocally resonant metamaterial features a domain exhibiting an anomalous cone (blue area). This cone is due to the presence of a delocalized mode with finite wave number k_R at 0 Hz. (d) A geometry that hosts such nonlocal elastic resonances down to 0 Hz.

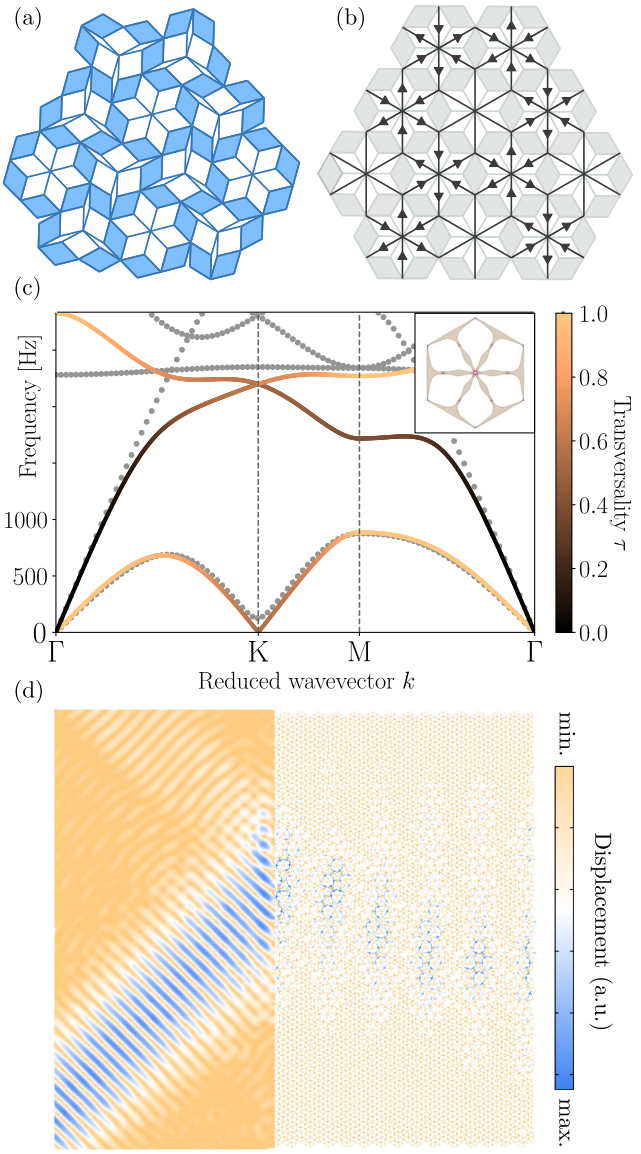

FIG. 2. (a) A zero-energy deformation mode of the structure of Fig. 1(d). (b) Corresponding graph overlaid on the undeformed geometry. (c) Dispersion relation along symmetry lines of the Brillouin zone, with solid lines corresponding to a spring-mass model and dots to a finite-element simulation with the inset geometry. Solid lines are colored according to the transversality of corresponding eigenmodes. (d) Finite-element simulation of a monochromatic Gaussian beam negatively refracted at the interface between an isotropic material (left) and this nonlocally resonant metamaterial (right).

zero-energy modes. Removing a sufficient number of rigid springs makes it possible for localized rigid motion to occur, typically leading to Guest-Hutchinson modes [35,36], which have 1D extension both in real space and k space [37]. Such modes cannot create anomalous dispersion cones, which are pinned to isolated points in k space. Instead, we seek a geometry hosting a finite number of mechanisms, and therefore a finite number of anomalous cones. In addition, inverse design necessitates a geometry complex enough to be tailorable. We thus need to go beyond the counterrotating squares geometry and turn to oligomodal metamaterials [38]. Indeed, oligomodal geometries are defined through their property of hosting a finite number of zero-energy modes that does not scale with system size. We must add another requirement, namely, that such modes be of the Bloch-wave form, with well-defined $\mathbf{k_R}$. The metamaterial of Fig. 1(d) qualifies, as we now demonstrate.

To do so, we use a convenient description of mechanisms in terms of directed graphs [38]. Concrete examples are detailed in the Supplemental Material [37]. In this method, one starts by drawing a graph with a vertex in every empty polygon enclosed by rigid springs (also known as a "linkage"). A second type of vertex is drawn on every point mass; we will refer to these as "hinges." We then draw edges connecting every linkage vertex to the surrounding hinges. To describe nontrivial rigid motions, arrows are drawn on each edge to depict relative rotation of the two neighboring rigid springs, with the number of arrows being proportional to the angular deformation. From a mechanical structure [Fig. 2(a)], we obtain a directed graph encoding angular

deformations [Fig. 2(b)]. Such deformations only entail local rotations and occur without stretching, consistent with their zero-frequency character.

Kinematics impose constraints on the allowed arrow configurations. First, all vertices are subject to arrow conservation, meaning that incoming and outgoing arrows must exactly balance each other; this reflects the fact that the sum of angles is invariant. Second, the vertices associated with linkages are subject to additional constraints encoding their mechanical degrees of freedom; for instance, vertices surrounded by three rigid springs are statically determined and can be erased along with their edges. Vertices of degree 4 possess 1 degree of freedom, meaning that fixing the arrow count on one edge determines the other three. In general, vertices of degree n have $n-3$ degrees of freedom. The precise arrow-drawing rule is obtained by linearizing the trigonometric relations between the angles of the linkage [38] or from symmetry considerations in simple cases. In general, this leads to vertices with unequal arrow weights, possibly noninteger. Therefore, the problem of finding nontrivial modes at zero frequency becomes combinatorial [39,40]; one needs to find all linearly independent arrow configurations that respect the aforementioned rules.

The directed graph of Fig. 2(b) was obtained by applying the combinatorial rules [Fig. 1(d)]; there, the unit-cell graph has been simplified to a vertex of degree 6. This equivalent vertex has 1 degree of freedom, which is drawn as alternating incoming and outgoing arrows. The combinatorial game goes like this: we draw an arrow on an arbitrary edge, say in the top-left cell of Fig. 2(b). This fixes five other edges through the kinematic vertex rule, but the remainder of the graph is not yet fully determined. We therefore need to choose the direction of another arrow in a neighboring cell, keeping arrow conservation in mind. In particular, this fixes the third arrow at any vertex shared by two neighboring unit cells and therefore determines the arrow distribution on that unit cell as well. The arrows then propagate over the whole graph coherently, yielding Fig. 2(b). Under the corresponding deformation mode, the structure of Fig. 1(d) is deformed into the one of Fig. 2(a). Since we had to fix two arrows, we see that the lattice has 2 mechanical degrees of freedom that act system-wide, i.e., two nonlocal resonances. We therefore expect the spectrum to host two anomalous cones at the wave vectors associated with these zero-energy modes. Consider their spatial periodicity, easily observed on the graph of Fig. 2(b); the deformation pattern repeats only after three cells in the horizontal direction. Since we can select the second mode as a mirror image of the first, our graph theory predicts anomalous cones that nucleate at zero frequency from the K and K' points of the Brillouin zone.

To verify this, we let the springs stretch again, allowing for oscillations at nonzero frequencies. Collecting the displacements of all point masses in a vector $\mathbf{u}$, we can describe such oscillations through the differential equation $\partial_t^2\mathbf{u} = \mathcal{D}\mathbf{u}$, where the dynamical matrix $\mathcal{D}$ encodes the effect of springs [36]. Connecting masses on opposite boundaries of the unit cell with phase-shifted springs to implement Floquet-Bloch boundary conditions, we compute a phononic band structure for a spring-mass model with the geometry of Fig. 1(d), with blue diamonds replaced by equivalent triangulated spring frames [37]. We see in Fig. 2(c) that an additional cone then emerges from the K point.

Let us discuss the impact of anomalous cones on waves. First, they induce domains of negative group velocity that extend from 0 Hz over a large bandwidth. Wave packets prepared on these domains are negatively refracted at interfaces with isotropic elastic media. As for wavelengths closer to Γ, they are positively refracted and split in longitudinal and transverse components. This phenomenon may be leveraged to filter wavelengths. To suppress positive refraction, one can pin the unit cell, thereby removing the cones near Γ [37]. At higher frequencies, a second feature stands out: the anomalous cone hybridizes with another one. For instance, in Fig. 2(c), it connects with transverse elastic waves. Interestingly, this hybridization creates a partial band gap in which only longitudinal waves are allowed. Other interesting band gaps arise by pretwisting the metamaterial; for instance, selecting Fig. 2(a) as the rest position can induce complete band gaps [37]. We identified gaps with relative bandwidth up to $(\Delta\omega/\omega) = 56\%$. Such graph-preserving pretwists also impact the speed of anomalous waves [37]. These examples show that a given graph model only fixes the location of the cones, defining a large family of nonlocally resonant metamaterials.

To validate these theoretical insights, we performed full-wave finite-element simulations. There, we use a realistic hinge design that favors bending over stretching [37,38] by combining a soft and a rigid material. Armed with these hinges, we reproduce the spring-mass band structure in Fig. 2(c) using a finite-element (COMSOL) eigenvalue study with Floquet-Bloch boundary conditions. The bimaterial unit-cell geometry is represented in the inset of Fig. 2(c) and [37]. The theoretical and numerical low-energy phonon branches are in close agreement, with the exception of a mass gap appearing at the K point. Such a gap is expected to arise as a result of the nonideal hinges; its size is determined by the finite hinge stiffness. Above 1500 Hz, the predictions of the finite-element method and theory start diverging; this reflects the fact that, while both models share the same underlying mechanism, the internal structure of their rigid elements differs greatly. Once such elements start to deform, the spectra diverge. Our spring-mass model captures the dynamics below this threshold. This illustrates the fact that several geometries can instantiate the same abstract mechanism, while their higher-frequency spectra generically differ. For further examples, see the Supplemental Material [37].

Next, we explicitly demonstrate that the phase and group velocities around the anomalous cone are opposite, in a numerical experiment directly probing the refraction of a monochromatic Gaussian beam at the interface between an isotropic medium and our nonlocally resonant metamaterial. The metamaterial domain consists of a hexagonal tiling of $29 \times 42 = 1218$ unit cells of the type depicted in the inset of Fig. 2(c). The result, presented in Fig. 2(d), clearly evidences the negative refraction of the beam, consistent with the strong nonlocality exhibited by the architected material [7,8]. Simultaneous positive refraction is suppressed because the incoming beam contains little energy near Γ. In the Supplemental Material [37], we report additional simulations over a wide-frequency range, finding a relative bandwidth of $(\Delta\omega/\omega_c) = 48\%$. Therefore, anomalous cones can have drastic consequences on wave propagation and be considered as a fundamental route to create metamaterials with broadband spatially dispersive effects.

Turning to experiments, we 3D printed a dual-material structure [Fig. 3(a) and [37]] approximating the lattice of Figs. 1(b) and 1(d). The white sections were printed with polyactic acid (PLA), whereas the orange sections forming the hinges were printed using a much more flexible thermopolyurethane (TPU) [37]. We then excited elastic waves with pseudorandom noise in a range of 10–1250 Hz in our 61-cell hexagonal sample using a shaker and measured the internal rotation of each unit cell through laser vibrometry. The vibrometer was placed at a 26° angle from the sample plane in order to favor in-plane velocity. Taking three measurement points per cell [green points in Fig. 3(e)] allowed us to construct a measure of internal rotation, namely, $\Omega := 2v_2 - v_1 - v_3$, where v_1 and v_3 were measured on the disconnected central triangles of the cell and v_2 in the center [37]. Figures 3(b)–3(d) depict spatial Fourier transforms of the results, superimposed with frequency contours obtained through the spring-mass model. Despite its simplified microarchitecture, this model agrees with the experimental data. Figure 3(b) clearly indicates a concentration of energy at the K and K' points at 106 Hz. As for Fig. 3(c), it shows how the anomalous cones open up with increasing frequency, progressively deforming into triangular contours. By 806 Hz, the cones have merged and the resulting elliptic contours are still in agreement with the model [Fig. 3(d)]; they converge to the M point at 888 Hz. This confirms the possibility of realizing nonlocally resonant elastic metamaterials, with a large bandwidth: here, the anomalous branch extends from 106 to 888 Hz.

The examples considered so far exhibited anomalous cones at highly symmetric points, and our method to find them remained heuristic. We want to go further and see whether inverse design is possible: how do we design a geometry exhibiting an anomalous cone at a specified location in k space?

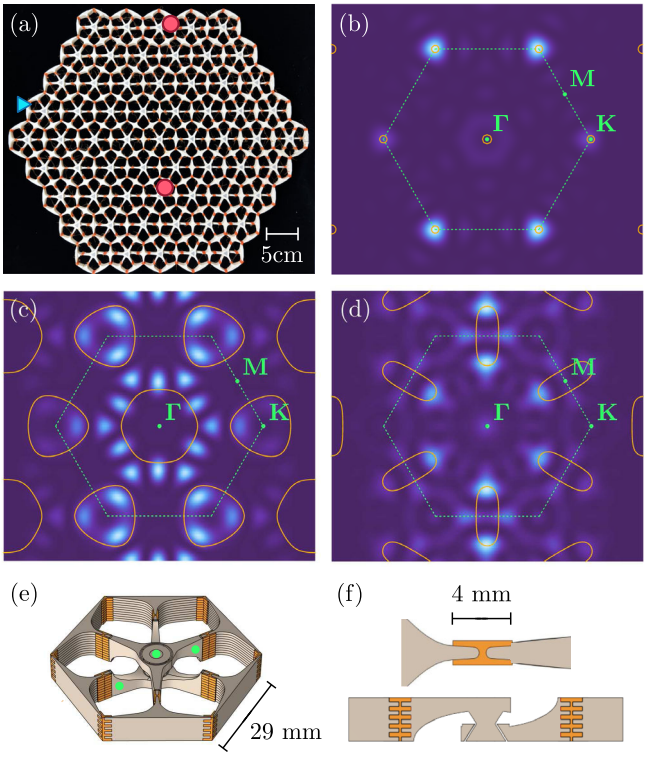

FIG. 3. Experimental validation. (a) 3D-printed sample, with fixed points denoted by red circles and excitation points by blue triangles. (b)–(d) Spatial Fourier transform of $|\Omega|^2$ at 106, 529 and 806 Hz, respectively. Solid yellow lines represent the isofrequency contours (first band) predicted by the spring-mass model. Green dashed lines mark the limits of the Brillouin zone, and symmetry points are labeled. (e) Geometry of the 3D-printed unit cell, with PLA regions in brown and TPU regions in orange. Measurement points are indicated in green. (f) Close-up of the hinge geometry and cross section of the unit cell.

Consider a combinatorially designed unit cell, for instance, the one of Fig. 4(a); it has an anomalous cone at the M point [37]. We want to move this anomalous cone to an arbitrary location in the two-dimensional k space. Therefore, we start by tuning two geometric parameters in the unit cell [the angles between the central links in Fig. 4(c)]. This generically frustrates the mechanism, by lifting symmetry-induced redundancies in the link constraints [37], thereby opening up a mass gap in the anomalous cone. To avoid this, we remove four constraints from the unit cell (three central bars and a triangle), as shown in Fig. 4(c).

We then invert the problem of determining the location of the anomalous cone: first, we enforce Floquet-Bloch boundary conditions by writing an arrow-conservation equation for every hinge connecting the unit cell to its neighbors. These equations can be collected in a matrix [37] whose kernel contains arrow configurations compatible with the target wave vector. Second, we compute the arrow rules for arbitrary values of the geometric parameters, which yields a nonlinear system of equations relating the arrow weights to the unit-cell geometry [37]. Finally,

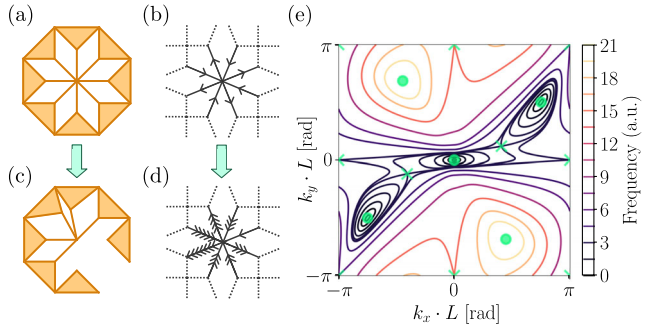

FIG. 4. Inverse design of anomalous cones. (a) Octagonal unit cell. (b) Associated vertex model. (c) Deformed unit cell, designed to exhibit an anomalous cone at an arbitrarily chosen location $(k_x, k_y) = (3\pi/4, \pi/2)$. (d) Graphical depiction of a vertex satisfying the target Floquet-Bloch boundary conditions. (e) Isofrequency contours of the first branch for geometry (c). Extrema are indicated with circles and saddle points with crosses.

we combine the boundary conditions and the geometric equations to obtain the desired unit-cell parameters. See the Supplemental Material [37] for explicit details of these computations.

Concretely, for $L \cdot (k_x, k_y) = (3\pi/4, \pi/2)$, the kernel of the arrow-conservation matrix contains a configuration approximated in Fig. 4(d) (the exact arrow weights are not integers). We then insert these weights in the geometric parameters equations [37], which we invert to obtain the desired metamaterial geometry [Fig. 4(c)]. This completes the process; we can verify that the corresponding spring-mass model exhibits an anomalous cone centered at $L \cdot (k_x, k_y) = (3\pi/4, \pi/2)$ in Fig. 4(e). Time-reversal symmetry implies that another cone lies at $L \cdot (k_x, k_y) = -(3\pi/4, \pi/2)$.

Nonlocally resonant metamaterials, which unify the present elastic metamaterials and interlaced wire media, also shed new light on another type of metamaterial: roton metamaterials [24–29,41]. Although based on a different physical mechanism, namely, long-range interactions, roton metamaterials also achieve wide domains of negative group velocity by leveraging a type of nonlocality. We have identified two ways in which nonlocal resonances can open a mass gap and acquire rotonlike dispersion, namely, through kinematic frustration or hinge design. Conversely, we surmise that electromagnetic rotons could be designed by perturbation of ideal interlaced wire media, either geometric or material in nature.

In conclusion, we introduced the notion of nonlocally resonant metamaterials, wherein anomalous dispersion cones originate from arbitrary points in k space, associated with sample-spanning resonances. We showed that such cones lead to band gaps, slow sound, and negative indices over a large bandwidth. We experimentally observed deep-subwavelength spatial dispersion in a 3D-printed nonlocally resonant elastic metamaterial. Finally, a directed-graph theory allowed us to inversely design anomalous cones.

A. B. and R. F. acknowledge funding from the Swiss National Science Foundation under Eccellenza Grant No. 181232 entitled "Ultra-compact wave devices based on deep subwavelength spatially dispersive effects."

*aleksi.bossart@epfl.ch
†romain.fleury@epfl.ch

[1] X. Zhou, X. Liu, and G. Hu, Elastic metamaterials with local resonances: An overview, Theor. Appl. Mech. Lett. **2**, 041001 (2012).
[2] C. T. Chan, J. Li, and K. H. Fung, On extending the concept of double negativity to acoustic waves, J. Zhejiang Univ.—Sci. A **7**, 24 (2006).
[3] H. Huang and C. Sun, Theoretical investigation of the behavior of an acoustic metamaterial with extreme Young's modulus, J. Mech. Phys. Solids **59**, 2070 (2011).
[4] A. Schuster, *An Introduction to the Theory of Optics* (E. Arnold & Company, London, 1924).
[5] H. Lamb, On Group—Velocity, Proc. London Math. Soc. **s2-1**, 473 (1904).
[6] H. H. Huang and C. T. Sun, Anomalous wave propagation in a one-dimensional acoustic metamaterial having simultaneously negative mass density and Young's modulus, J. Acoust. Soc. Am. **132**, 2887 (2012).
[7] D. Forcella, C. Prada, and R. Carminati, Causality, Nonlocality, and Negative Refraction, Phys. Rev. Lett. **118**, 134301 (2017).
[8] P. A. Belov, R. Marqués, S. I. Maslovski, I. S. Nefedov, M. Silveirinha, C. R. Simovski, and S. A. Tretyakov, Strong spatial dispersion in wire media in the very large wavelength limit, Phys. Rev. B **67**, 113103 (2003).
[9] V. G. Veselago, The electrodynamics of substances with simultaneously negative values of ϵ and μ, Sov. Phys. Usp. **10**, 509 (1968).
[10] J. B. Pendry, Negative Refraction Makes a Perfect Lens, Phys. Rev. Lett. **85**, 3966 (2000).
[11] J. B. Pendry, A. J. Holden, W. J. Stewart, and I. Youngs, Extremely Low Frequency Plasmons in Metallic Mesostructures, Phys. Rev. Lett. **76**, 4773 (1996).
[12] J. Pendry, A. Holden, D. Robbins, and W. Stewart, Magnetism from conductors and enhanced nonlinear phenomena, IEEE Trans. Microw. Theory Techn. **47**, 2075 (1999).
[13] Z. Liu, X. Zhang, Y. Mao, Y. Y. Zhu, Z. Yang, C. T. Chan, and P. Sheng, Locally resonant sonic materials, Science **289**, 1734 (2000).
[14] N. Fang, D. Xi, J. Xu, M. Ambati, W. Srituravanich, C. Sun, and X. Zhang, Ultrasonic metamaterials with negative modulus, Nat. Mater. **5**, 452 (2006).
[15] Z. Yang, J. Mei, M. Yang, N. H. Chan, and P. Sheng, Membrane-Type Acoustic Metamaterial with Negative Dynamic Mass, Phys. Rev. Lett. **101**, 204301 (2008).
[16] C. Z. Fan, Y. Gao, and J. P. Huang, Shaped graded materials with an apparent negative thermal conductivity, Appl. Phys. Lett. **92**, 251907 (2008).
[17] J. Christensen, M. Kadic, O. Kraft, and M. Wegener, Vibrant times for mechanical metamaterials, MRS Commun. **5**, 453 (2015).

[18] K. Bertoldi, V. Vitelli, J. Christensen, and M. van Hecke, Flexible mechanical metamaterials, Nat. Rev. Mater. **2**, 11 (2017).
[19] D. Yu, Y. Liu, H. Zhao, G. Wang, and J. Qiu, Flexural vibration band gaps in Euler-Bernoulli beams with locally resonant structures with two degrees of freedom, Phys. Rev. B **73**, 5 (2006).
[20] C. L. Kane and T. C. Lubensky, Topological boundary modes in isostatic lattices, Nat. Phys. **10**, 39 (2014).
[21] A. S. Meeussen, J. Paulose, and V. Vitelli, Geared Topological Metamaterials with Tunable Mechanical Stability, Phys. Rev. X **6**, 041029 (2016).
[22] R. Lakes, Foam structures with a negative Poisson's ratio, Science **235**, 1038 (1987).
[23] G. W. Milton and A. V. Cherkaev, Which elasticity tensors are realizable?, J. Eng. Mater. Technol. **117**, 483 (1995).
[24] Z. Zhou, S. Huang, D. Li, J. Zhu, and Y. Li, Broadband impedance modulation via non-local acoustic metamaterials, Natl. Sci. Rev. **9**, nwab171 (2022).
[25] Y. Chen, M. Kadic, and M. Wegener, Roton-like acoustical dispersion relations in 3D metamaterials, Nat. Commun. **12**, 3278 (2021).
[26] J. A. Iglesias Martínez, M. F. Groß, Y. Chen, T. Frenzel, V. Laude, M. Kadic, and M. Wegener, Experimental observation of roton-like dispersion relations in metamaterials, Sci. Adv. **7**, eabm2189 (2021).
[27] G. J. Chaplain, I. R. Hooper, A. P. Hibbins, and T. A. Starkey, Reconfigurable Elastic Metamaterials: Engineering Dispersion with beyond Nearest Neighbors, Phys. Rev. Appl. **19**, 044061 (2023).
[28] L. Landau, Theory of the superfluidity of helium II, Phys. Rev. **60**, 356 (1941).
[29] R. P. Feynman and M. Cohen, Energy spectrum of the excitations in liquid helium, Phys. Rev. **102**, 1189 (1956).
[30] W.-J. Chen, B. Hou, Z.-Q. Zhang, J. B. Pendry, and C. T. Chan, Metamaterials with index ellipsoids at arbitrary k-points, Nat. Commun. **9**, 2086 (2018).
[31] D. Sakhno, E. Koreshin, and P. A. Belov, Longitudinal electromagnetic waves with extremely short wavelength, Phys. Rev. B **104**, L100304 (2021).
[32] A. P. Giddy, M. T. Dove, G. S. Pawley, and V. Heine, The determination of rigid-unit modes as potential soft modes for displacive phase transitions in framework crystal structures, Acta Crystallogr. Sect. A **49**, 697 (1993).
[33] M. T. Dove, Theory of displacive phase transitions in minerals, Am. Min. **82**, 213 (1997).
[34] D. Z. Rocklin, Bryan Gin-ge Chen, M. Falk, V. Vitelli, and T. C. Lubensky, Mechanical Weyl Modes in Topological Maxwell Lattices, Phys. Rev. Lett. **116**, 135503 (2016).
[35] S. D. Guest and J. W. Hutchinson, On the determinacy of repetitive structures, J. Mech. Phys. Solids **51**, 383 (2003).
[36] T. C. Lubensky, C. L. Kane, X. Mao, A. Souslov, and K. Sun, Phonons and elasticity in critically coordinated lattices, Rep. Prog. Phys. **78**, 073901 (2015).
[37] See Supplemental Material at http://link.aps.org/supplemental/10.1103/PhysRevLett.130.207201 for (I) Introduction to the directed-graph method, (II) impact of pretwisting on band structure, (III) bandwidth of negative refraction, (IV) prototyping details, and (V) details of inverse-design method.
[38] A. Bossart, D. M. J. Dykstra, J. van der Laan, and C. Coulais, Oligomodal metamaterials with multifunctional mechanics, Proc. Natl. Acad. Sci. U.S.A. **118**, e2018610118 (2021).
[39] C. Coulais, E. Teomy, K. de Reus, Y. Shokef, and M. van Hecke, Combinatorial design of textured mechanical metamaterials, Nature (London) **535**, 529 (2016).
[40] A. S. Meeussen, E. C. Oğuz, Y. Shokef, and M. v. Hecke, Topological defects produce exotic mechanics in complex metamaterials, Nat. Phys. **16**, 307 (2020).
[41] J. Kishine, A. S. Ovchinnikov, and A. A. Tereshchenko, Chirality-Induced Phonon Dispersion in a Noncentrosymmetric Micropolar Crystal, Phys. Rev. Lett. **125**, 245302 (2020).